Mass transfer and electrolyte flow during electrodeposition on a conically shaped electrode under the influence of a magnetic field

Huang, M.; Marinaro, G.; Yang, X.; Fritzsche, B.; Lei, Z.; Uhlemann, M.; Eckert, K.; Mutschke, G.;

Originally published:

June 2019

Journal of Electroanalytical Chemistry 842(2019), 203-213

DOI: https://doi.org/10.1016/j.jelechem.2019.04.043

Perma-Link to Publication Repository of HZDR:

https://www.hzdr.de/publications/Publ-29127

Mass transfer and electrolyte flow during electrodeposition on a conically shaped electrode under the influence of a magnetic field

M. Huang, G. Marinaro, X. Yang, B. Fritzsche, Z. Lei, M. Uhlemann, K. Eckert, G. Mutschke

PII: S1572-6657(19)30307-8
DOI: https://doi.org/10.1016/j.jelechem.2019.04.043
Reference: JEAC 13083

To appear in: *Journal of Electroanalytical Chemistry*

Received date: 25 January 2019
Revised date: 17 April 2019
Accepted date: 17 April 2019

Please cite this article as: M. Huang, G. Marinaro, X. Yang, et al., Mass transfer and electrolyte flow during electrodeposition on a conically shaped electrode under the influence of a magnetic field, Journal of Electroanalytical Chemistry, https://doi.org/10.1016/j.jelechem.2019.04.043

Mass transfer and electrolyte flow during electrodeposition on a conically shaped electrode under the influence of a magnetic field

M. Huang[a,1], G. Marinaro[a,b,1], X. Yang[a,b], B. Fritzsche[b], Z. Lei[a,b], M. Uhlemann[c], K. Eckert[a,b], G. Mutschke[a,*]

[a]Helmholtz-Zentrum Dresden-Rossendorf (HZDR), Institute of Fluid Dynamics, 01328 Dresden, Germany
[b]Technische Universität Dresden, Institute of Process Engineering, 01069 Dresden, Germany
[c]IFW Dresden, Institute of Complex Materials, 01069 Dresden, Germany

Abstract

The electrodeposition of copper on a conically shaped diamagnetic electrode was studied under the influence of a vertical magnetic field. Numerical simulations combined with measurements of the velocity and the concentration field were conducted to provide understanding of the influence of the Lorentz force on the deposition process. The secondary flow caused by the magnetic field is directed downward along the cone surface and thus supporting conical growth. Since the cathode is placed at the bottom of the electrochemical cell, natural convection is counteracting the influence of the Lorentz force. However, the different time scales of both forces involved allow to utilize the beneficial influence of the Lorentz force, e.g. in pulsed deposition regimes.

Keywords: copper electrodeposition, magnetic field, surface-structured electrode, Mach-Zehnder interferometry, shadowgraphy, numerical simulation

[1] Both authors contributed equally to this work.
[*] Corresponding author. E-Mail address: g.mutschke@hzdr.de

1 Introduction

Rapid development in micro- and nanoelectronics tends towards miniaturization of functional structures with high aspect ratios, whereby conical structures at length scales from micrometer to nanometer have gained much attention due to their numerous applications in areas including microscopies, super-hydrophobic and electrocatalytic materials [1] [2] [3]. Due to their excellent electrocatalytic activity, nano-cone arrays are particularly attractive for water electrolysis. It was reported that the special nano-conical geometry of the electrode promotes the hydrogen evolution reaction by preventing bubble coalescence and by favouring bubble detachment [4] [5] and also increases the electrochemically active surface area [3] [6] [7]. Among the various methods of synthesizing arrays of micro- and nano-structured cones, electrochemical deposition techniques have gained much attention due to their simplicity, their low-cost and their ability to fabricate highly ordered structures [8] [9] [10]. Enhanced transport of the electroactive ions towards the tip of a conical cathode by migration and diffusion provides a higher current density at the tip compared to other regions of the cathode [11] [12] [13]. This non-uniform distribution of the current density results in a higher deposition rate at the tip of the cone, so that the aspect ratio of the growing cone increases with time. Meanwhile, the effects of magnetic fields on the structured electrodeposition of metal have been a matter of interest for the past decades (for a recent review, see [10]). It is well known that the influence of magnetic fields on the mass transport and on the morphology of the deposited layers can be attributed to the action of the Lorentz force and the magnetic gradient force [14] [15] [16]. As the magnetic field applied in the present study is a quasi-homogeneous field, the magnetic gradient force will not be discussed here. Additionally, natural convection is usually involved in the deposition process due to the concentration gradients arising during deposition and the associated density gradients near the cathode. **Figure 1** schematically shows the flows induced by the Lorentz force and the buoyancy force near a conical cathode. The Lorentz force $\boldsymbol{f}_{\mathrm{L}}$ is resulting from the vertical magnetic field $\boldsymbol{B}$ and the radial component of the current density and is creating an azimuthal flow around the cone [17] [18]. The centrifugal force generated from this primary flow gives rise to a secondary flow which brings fresh electrolyte downwards to the tip of the cone. Apart from the magnetic force, the electrochemical reaction taking place at the cathode causes lower electrolyte density in this area, which gives rise to natural convection. As the cathode is placed at the bottom of the electrochemical cell, the buoyancy force near the cathode tends to bring the electrolyte upwards, which in interaction with the Lorentz force will generate a complex three-dimensional flow.

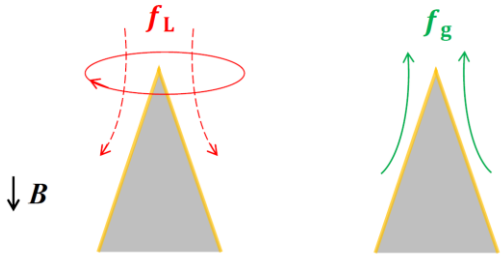

Figure 1: Flow (schematically) induced by the Lorentz force $\boldsymbol{f}_{\mathrm{L}}$ (primary and secondary flow drawn by solid and dashed lines, respectively), and the buoyancy force $\boldsymbol{f}_{\mathrm{g}}$ near the conical cathode.

This flow can be expected to influence the mass transfer on the cathode. It is therefore possible to control the electrodeposition process by properly adjusting the magnetic fields imposed on the electrochemical cell [16] [19] [20]. This paper aims to investigate the electrodeposition process on a single conically shaped copper electrode at millimeter length scale under the influence of a vertical magnetic field. This should provide a basic understanding of the flow and the mass transfer at conical structures and contribute to future investigations on arrays of cones towards nanostructures, which upon reduction of the length scales have shown novel physical and chemical properties [21]. In the present work, the velocity and the concentration field near the conical cathode were studied in detail by measurements and by numerical simulations. The electrolyte flow was visualized by shadowgraphy with application of particle tracking algorithm, and the concentration field was measured by a Mach-Zehnder interferometer. Numerical simulations were conducted to compare with the measurements and to deliver further detailed information on the deposition process.

2 Materials and methods

2.1 Experimental

Cone-shaped copper cathodes were fabricated by a Computerized Numerical Control (CNC) technique (**Figure 2(a)**). The cone diameter was 2 mm, and the tip angle was 60 degrees (**Figure 2(b)**). The surface exposed to the electrolyte is 6.22 mm^2. The cone was electrochemically polished and sputtered with a protective film of gold (100 nm). It should be noticed that a small part of the tip (height=0.13 mm) is truncated due to fabrication details (**Figure 2(b)**), resulting in a cone height of 1.6 mm in total. The influence of such imperfectness of the cone shape is discussed in Section 3.4. Cuvettes were purchased from Hellma Analytics and made of Quartz SUPRASIL. The height was 45 mm and the inner cross section was 10x10 mm^2. A cylindrical NdFeB magnet (height=20 mm, diameter=20 mm) magnetized downwards along its axis was placed below the cone at a distance of about 10 mm between the upper surface of the magnet and the bottom of the cone (**Figure 2(c)**), providing a magnetic field of 0.06 T near the cone, as measured by a Gaussmeter (Type Fieldmeter H2 from MAGMESS Magnet-Messtechnik Jürgen Ballanyi e.K.). An aqueous solution of 0.1 M $CuSO_4$ was prepared as the electrolyte, having a pH value of 4.2. A potentiostat (CH Instrument) was set in galvanostatic mode for the electrodeposition. A Platinum wire (ALS Co.) of 0.5 mm diameter was used as counter-electrode and placed vertically in the upper part of the cell.

The concentration measurements were carried out using a Mach-Zehnder interferometer (the setup is illustrated in Figure 2(c)). The fringe pattern variations obtained were analyzed by an in-house Matlab code which is applying a wavelet transformation to obtain the refractive index map [22] [23] [24] [25]. Then, the gradient of concentration was calculated by the help of calibration measurements.

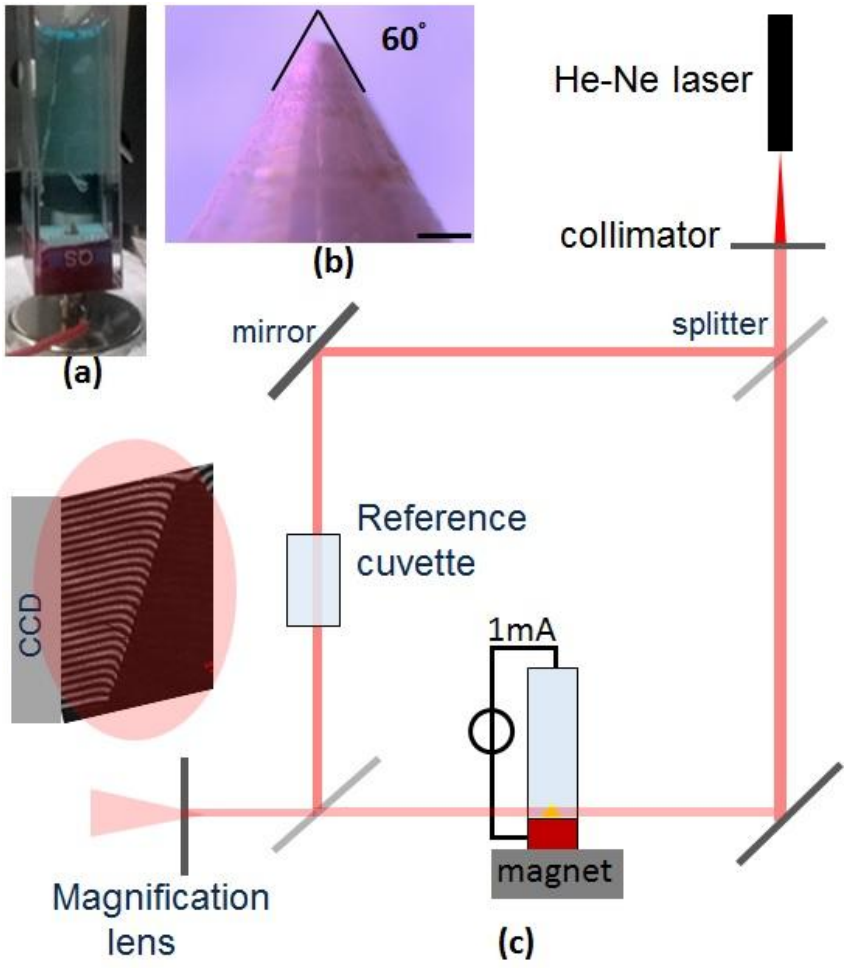

Figure 2: (a) Image of the cuvette with $CuSO_4$ electrolyte, magnet and conical electrode. (b) Optical image of the cone. The scale bar is 200 μm. (c) Sketch of Mach-Zehnder setup.

A similar setup as for Mach-Zehnder interferometry was used for tracking particles during electrodeposition. Monodisperse spherical polystyrene (PS) particles, with a size of 36 μm, were added to the electrolyte. The cuvette was illuminated by a laser (Model 32734 from Research Electro-Optics, Inc.), and shadowgraph frames were recorded by a camera placed on the back. Images were acquired during 90 s of electrodeposition and analyzed by using an in-house code written in Matlab and extended from previous work [26]. Both interferometry and shadowgraphy images were acquired by using a COHU CMOS camera (Model 7812-2000, 1280 x 1024 effective pixels) at a speed of 10 frames/second and a field of view of about 5x5 mm^2. In all experiments, a constant cell current of 1 mA was applied, corresponding to a mean current density of j=16 mA/cm^2 at the cone.

2.2 Numerical

The numerical model applied in the simulations is described in detail in [17]. The velocity of the electrolyte is given by the incompressible Navier-Stokes-equation:

$$\rho\left[\frac{\partial \boldsymbol{u}}{\partial t}+(\boldsymbol{u}\cdot\nabla)\boldsymbol{u}\right]=-\nabla p+\eta\Delta\boldsymbol{u}+\boldsymbol{f}_{\mathbf{L}}+\boldsymbol{f}_{\mathbf{g}} \tag{1}$$

combined with the incompressibility constraint $\nabla\cdot\boldsymbol{u}=0$, where ρ, p and η denote the density, the pressure, and the dynamic viscosity of the electrolyte, respectively. The Lorentz force $\boldsymbol{f}_{\mathbf{L}}=\boldsymbol{j}\times\boldsymbol{B}$ is given by the vector product of the current density $\boldsymbol{j}$ and the magnetic flux density $\boldsymbol{B}$ and induces a magnetohydrodynamic (MHD) flow of the electrolyte. Density variations near the electrodes give rise to the buoyancy force $\boldsymbol{f}_{\mathbf{g}}=\boldsymbol{g}(\rho-\rho_0)$, where $\boldsymbol{g}=[0,-9.81,0]\ \mathrm{m/s^2}$ is the gravitational acceleration, and $\rho_0=1014\ \mathrm{kg/m^3}$ is the bulk density [27]. For small density variations, the Boussinesq approximation can be applied [17], where the density in Equation (1) is taken to be the constant bulk density ρ_0, and the buoyancy force takes the form of $\boldsymbol{f}_{\mathbf{g}}=\rho_0\boldsymbol{g}\sum_i\beta_i\left(c_i-c_i^0\right)$. Here c_i^0 denotes the bulk concentration of each species, c_i and β_i are the concentration and the volume expansion coefficient of each species, respectively. As a binary electrolyte is used, it holds $c_{\mathrm{Cu^{2+}}}=c_{\mathrm{SO_4{}^{2-}}}$ due to electrical neutrality of the electrolyte, and the index *i* may be omitted (electrolyte concentration denoted by *c*). The buoyancy force is thereby modified to $\boldsymbol{f}_{\mathbf{g}}=\rho_0\boldsymbol{g}\beta_{\mathrm{sol}}(c-c^0)$ with $\beta_{\mathrm{sol}}=1.6\times10^{-4}\ \mathrm{m^3/mol}$ [27] denoting the volume expansion coefficient of the electrolyte. As boundary condition, the velocity has to satisfy the no-slip condition $\boldsymbol{u}=0$ at the cell walls and at both electrodes.

The transport of the chemical species is given by the Nernst-Planck equation:

$$\frac{\partial c_i}{\partial t}+(\boldsymbol{u}\cdot\nabla)c_i=z_iF\frac{D_i}{RT}\nabla\cdot(c_i\nabla\phi)+D_i\Delta c_i \tag{2}$$

with z_i and D_i being the charge number and the diffusion coefficient of species i ($D_{\mathrm{Cu^{2+}}}=0.564\times10^{-9}\ \mathrm{m^2/s}$, $D_{\mathrm{SO_4{}^{2-}}}=1.004\times10^{-9}\ \mathrm{m^2/s}$ [28]). F, R, T and ϕ further denote the Faraday constant, the universal gas constant, the temperature and the electric potential in the electrolyte, respectively. In order to close Equation (2), conservation of charge $\nabla\cdot\boldsymbol{j}=0$ is implemented. The current density $\boldsymbol{j}$ consists of a migration part and a diffusion part of the transport of the ions in the electrolyte and is defined as

$$\boldsymbol{j}=-F^2\nabla\phi\sum_i z_i^2\frac{D_i}{RT}c_i-F\sum_i z_iD_i\nabla c_i \tag{3}$$

Due to the electric insulation, the normal current density has to vanish on the electrically passive walls. The normal flux of the electrically passive $\mathrm{SO_4^{2-}}$ ion is zero on all the walls as well as on the electrodes, as it does not take part in the chemical reaction. The normal flux of the electrically active $\mathrm{Cu^{2+}}$ ion is zero on passive walls and has to satisfy the condition of the electrode kinetics, which is expressed by the Butler-Volmer equation on the electrodes [28] [29]:

$$j=j_0\left(\frac{c_{\mathrm{Cu^{2+}}}}{c^0_{\mathrm{Cu^{2+}}}}\right)^{\gamma}\left[exp\left(\frac{\alpha_{\mathrm{a}}F}{RT}\eta_{\mathrm{s}}\right)-exp\left(\frac{-\alpha_{\mathrm{c}}F}{RT}\eta_{\mathrm{s}}\right)\right] \tag{4}$$

Here α_a,α_c are the transfer coefficients, where the charge number is already incorporated, γ is the slope of a logarithmic plot of exchange current density vs. concentration [30], and j_0 is the base value of the

exchange current density. $\eta_s = \phi_e - \phi - \phi_{eq}$ denotes the surface overpotential, which is defined as the potential of the electrode (relative to the solution) minus the value at equilibrium. As copper electrodes are assumed in the simulation, the equilibrium potential ϕ_{eq} corresponds to 0 V. As the magnetic field has only a very small effect on the kinetic parameters [31], these are obtained from the data available for the case without magnetic field [30] [32] [33] [34]. For the 0.1 M $CuSO_4$ solution under study here it reads: $j_0 = 1\ \mathrm{mA/m^2}$, $\alpha_a = 1.5$, $\alpha_c = 0.5$, $\gamma = 0.42$.

By virtue of the axial symmetry of the conical electrode, 2D axisymmetric simulations were performed using the finite element code Comsol [35]. The computational domain is shown in **Figure 3(a)**. The cell dimensions correspond to the aforementioned experimental setup. The cell voltage is properly adjusted at each instant of time of the transient simulations such as to provide a constant cell current of 1 mA. The resulting average current density at the anode and at the cathode are 1.3 mA/cm^2 and 16 mA/cm^2, respectively. The cylindrical permanent magnet is placed below the electrochemical cell such that its vertical center line coincides with the symmetry axis of the cell. By neglecting the electromagnetic induction, the magnetic field is given by the Maxwell equations and the constitutive relation as follows:

$$\nabla \cdot \boldsymbol{B} = 0, \nabla \times \boldsymbol{H} = 0 \quad (5)$$

$$\boldsymbol{B} = \mu_0(\boldsymbol{H} + \boldsymbol{M}) \quad (6)$$

Here $\boldsymbol{B}$, $\boldsymbol{H}$, $\boldsymbol{M}$, μ_0 denote the magnetic flux density, the magnetic field strength, the magnetization of the material, and the vacuum permeability, respectively. As mentioned above, the permanent magnet induces a magnetic field magnitude of about 0.06 T near the copper cone. **Figure 3(a**) visualizes the distribution of the magnetic induction in the cell (black arrows). **Figure 3(b)** shows in more detail the magnitude of the vertical and horizontal components of the magnetic flux density near the cone. The magnetic field is mainly directed vertically, as the horizontal component of the magnetic flux density is shown to be much smaller than the vertical component, especially near the vertical center line (r<1 mm). The vertical component of the magnetic flux density decreases only slightly with increasing r- and z-coordinates. As the dimensions of the magnet are large compared to the cone size, a quasi–homogeneous vertical magnetic field near the cone is obtained.

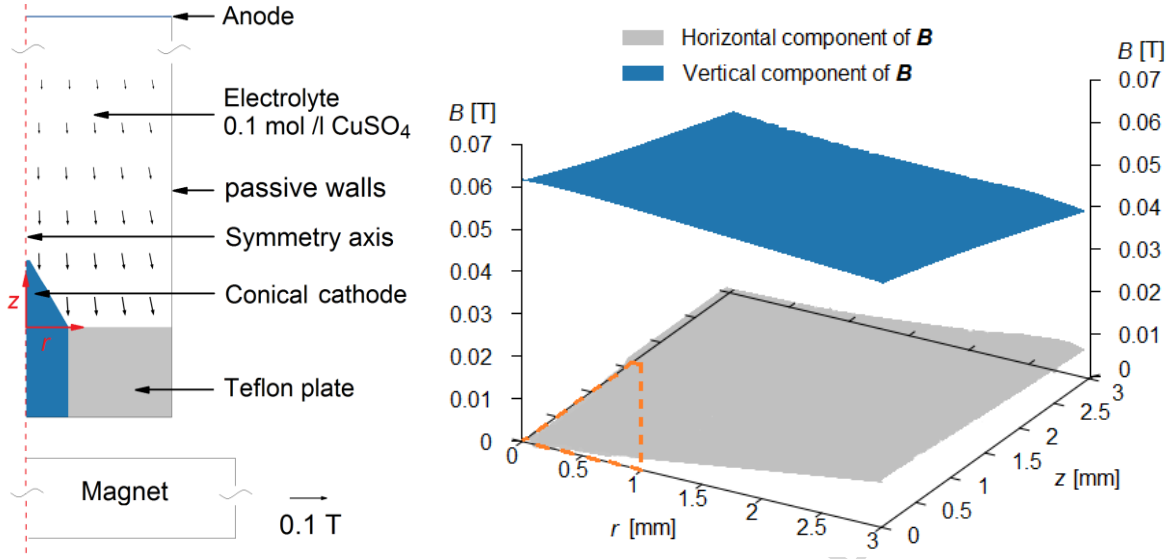

Figure 3: (a) Sketch of the computational domain. The coordinates *r* and *z* denote the radial and vertical coordinates, and the red dashed line is representing the symmetry axis. Scales are modified for better visibility. Further shown are the magnetic flux density vectors in the cell. (b) Distribution of the magnitude of the vertical and horizontal components of the magnetic flux density *B* near the cone, the position of which is marked by orange dashed lines.

Transient simulations were conducted to study the temporal behavior of the deposition process. The simulation initially starts from a homogenous state, i.e. $c_i(t=0) = c_i^0 = 0.1$ M. The initial velocity of the electrolyte $\boldsymbol{u}(t=0)$ is zero.

The unstructured grids used in the simulations were refined near the boundaries in order to adequately resolve the concentration and velocity boundary layers in these regions. According to the results of a mesh independence study, an unstructured mesh with 0.56 Mio. elements and an element length of 2 µm along the cell boundaries was selected for the following simulations. It was further found in a separate numerical study that concentration-related variations of the density and the viscosity only have a minor influence on the results. In order to simplify the calculations and to reduce the computational effort, constant fluid properties in combination with the Boussinesq approximation have been applied.

3 Results and Discussion

3.1 Concentration

It should be noticed that the concentration data obtained from the measurements by the Mach-Zehnder-Interferometer are averaged in direction of the laser beam. The simulation results therefore need to be processed correspondingly to allow a direct comparison between simulation and experiment. In the following, the y direction denotes the laser direction of the Mach-Zehnder-Interferometer with respect to

the Cartesian coordinate system $x - y - z$. The Abel transform is used to project the axially symmetric concentration field to a 2D plane orthogonal to the laser direction [36]:

$$c_{avg}(x,z) = 2\int_{y}^{\infty} \frac{c(r,z)rdr}{\sqrt{r^2 - x^2}} \tag{7}$$

Here, r and z denote the radial and the vertical coordinate in the cylindrical coordinate system introduced earlier. The so-calculated averaged concentration variation $\Delta c = c_{avg} - c^0$ with respect to the initial electrolyte concentration c^0 is compared with the experimental result in **Figure 4**. In the initial phase of the deposition at 5 s, concentration variations only exist near the cone surface. Copper ions are continuously consumed at the cathode with ongoing deposition, so the concentration boundary layer and the associated density variations near the cone become more pronounced in time. The latter gives rise to an upward buoyancy flow, which becomes visible at 10 s in the advection of the concentration boundary layer above the cone tip along the vertical center line. When comparing the concentration distribution at times 10 s and 30 s, only slight differences exist, indicating that the concentration boundary layer has reached a quasi-steady state. Such initial transient and subsequent quasi-steady state was also reported in [37]. Overall, a good qualitative agreement between simulation and experiment can be stated. In order to compare the results quantitatively, two monitoring lines were depicted. The concentration profiles along a horizontal line 0.4 mm above the cone tip (*z*=2 mm) and a line perpendicular to the cone surface at half height of the cone are presented for different instants of time in **Figure 5**. A moving average was applied to the noisy experimental data. Despite slight differences between the simulation and the experimental data, both results are in good agreement, and also the temporal behavior of the concentration boundary layer nicely coincides. At time 30 s, when the concentration field near the cone has reached a quasi-steady state, the thickness of the concentration boundary layer is about 0.24 mm at the monitoring line above the cone tip and about 0.12 mm at half height of the cone.

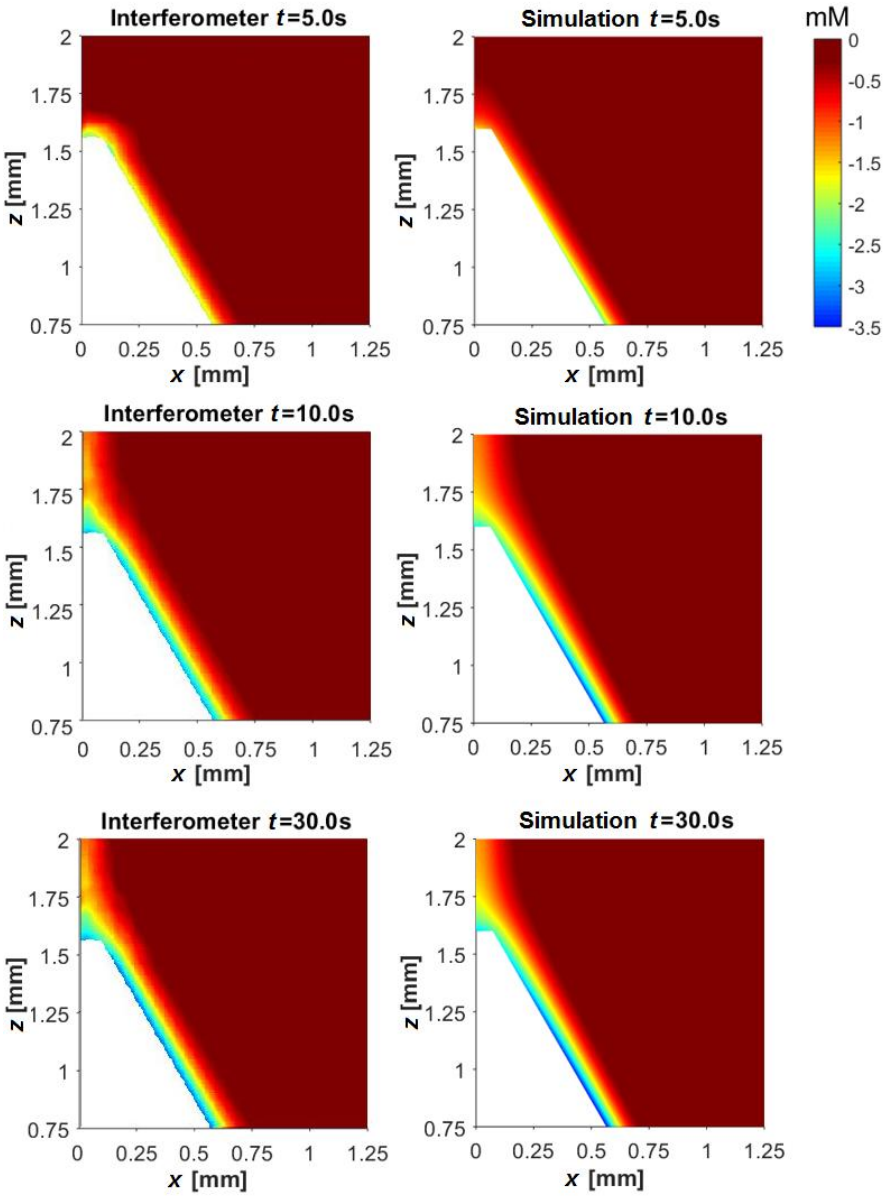

Figure 4: Comparison of the averaged concentration variation Δc near the cathode at different instants of time. Left: experiment, right: simulation.

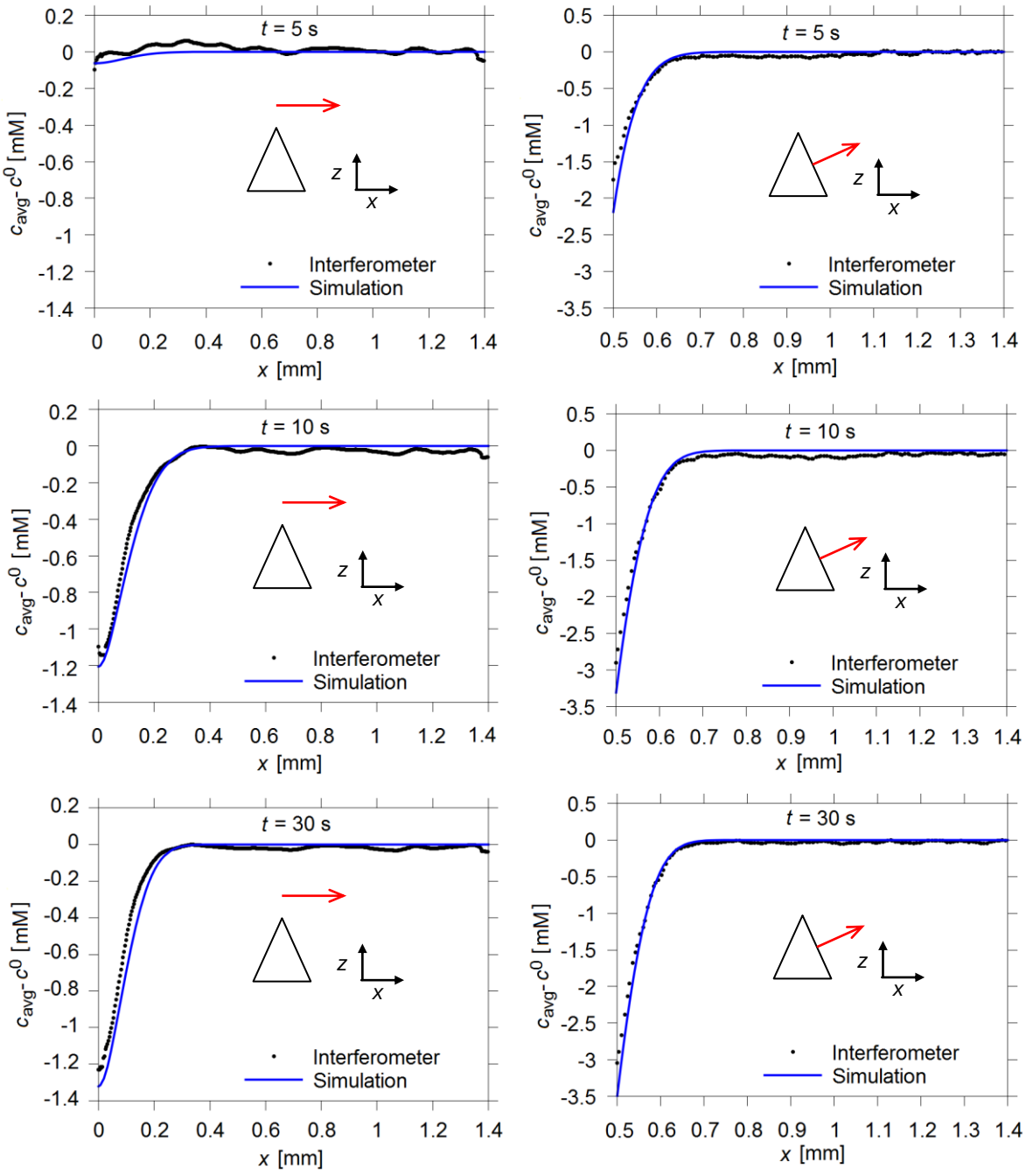

(a) (b)

Figure 5: Averaged concentration variation Δc from experiment and simulation at the horizontal (a) and the electrode-normal (b) monitoring line at different instants of time. The red arrows indicate the location and the direction of the monitoring lines.

3.2 Velocity

First, the amplitudes of the different volume forces involved are estimated to get a first hint on the flow regime in the cell. The ratio of Lorentz and buoyancy force can be calculated as follows [16]:

$$R_{\mathrm{MHD}} = \frac{f_{\mathrm{L}}}{\left|f_{\mathrm{g}}\right|} = \frac{jB_0}{\left|\rho_0 \beta g (c_{\mathrm{Cu^{2+}}} - c^0_{\mathrm{Cu^{2+}}})\right|} \tag{8}$$

Here the concentration $c_{\mathrm{Cu^{2+}}}$ is set to be 0 mM by assuming a limiting current regime. The characteristic magnetic induction B_0 is 0.06 T, and the characteristic current density is set to be the averaged cathode current density of 16 mA/cm^2. The so-calculated value of R_{MHD} amounts to about 0.06, indicating that the electrolyte flow might be dominated by the buoyancy force when the steady state has been reached. However, it should be noted that the amplitudes of both forces do vary in space and time, which makes a detailed investigation necessary. The magnitude of the azimuthal and meridional components of the velocity and the 3D velocity vectors obtained from the numerical simulations are shown in **Figure 6**. The azimuthal flow induced by the Lorentz force after beginning of the deposition process rapidly approaches a quasi-steady state, as seen already at time 5 s. This azimuthal flow is limited to the region near the cone, where the bending of electric field lines results in a radial component of the current density, which together with the vertical magnetic field generates the Lorentz force. In comparison, the buoyancy flow develops more slowly (see below), as with ongoing deposition the development of the concentration gradients near the cathode proceeds. This flow is pointing upward and is counteracting the secondary flow induced by the Lorentz force that is directed downward. As can be seen in **Fig. 6**, after 10 s, the meridional flow is dominated by the buoyancy force and a related upward flow above the tip of the cone, which in magnitude even exceeds the azimuthal velocity. This upward flow originates at the foot of the cone and continues with a parallel flow along the cone, which dampens the local mass transfer in the upper part of the cone, visible in a thicker concentration boundary layer in this region, as shown in **Figure 4**.

In order to describe the interplay of Lorentz force and buoyancy force in more detail, in the following the magnitudes of both forces averaged over the electrochemical cell are considered. The temporal behavior of the ratio between both averaged forces $f_{\mathrm{L,avg}}/f_{\mathrm{g,avg}}$ in the start-up phase of the deposition is shown in **Figure 7**. Also shown is the vertical velocity at a monitoring point 1 mm above the tip of the cone. As can be seen, the vertical velocity at the monitoring point changes its sign at about 5 s, suggesting that for later instants of time the previously downward directed flow dominated by the Lorentz force is converted into an upward flow dominated by the buoyancy force. This is in good agreement with the fact that the ratio between the averaged Lorentz force and buoyancy force is larger than one at the beginning but continuously reduces in time and sinks below one also at about 5 s. The analysis of the forces performed can therefore nicely explain the development of the electrolyte flow pattern.

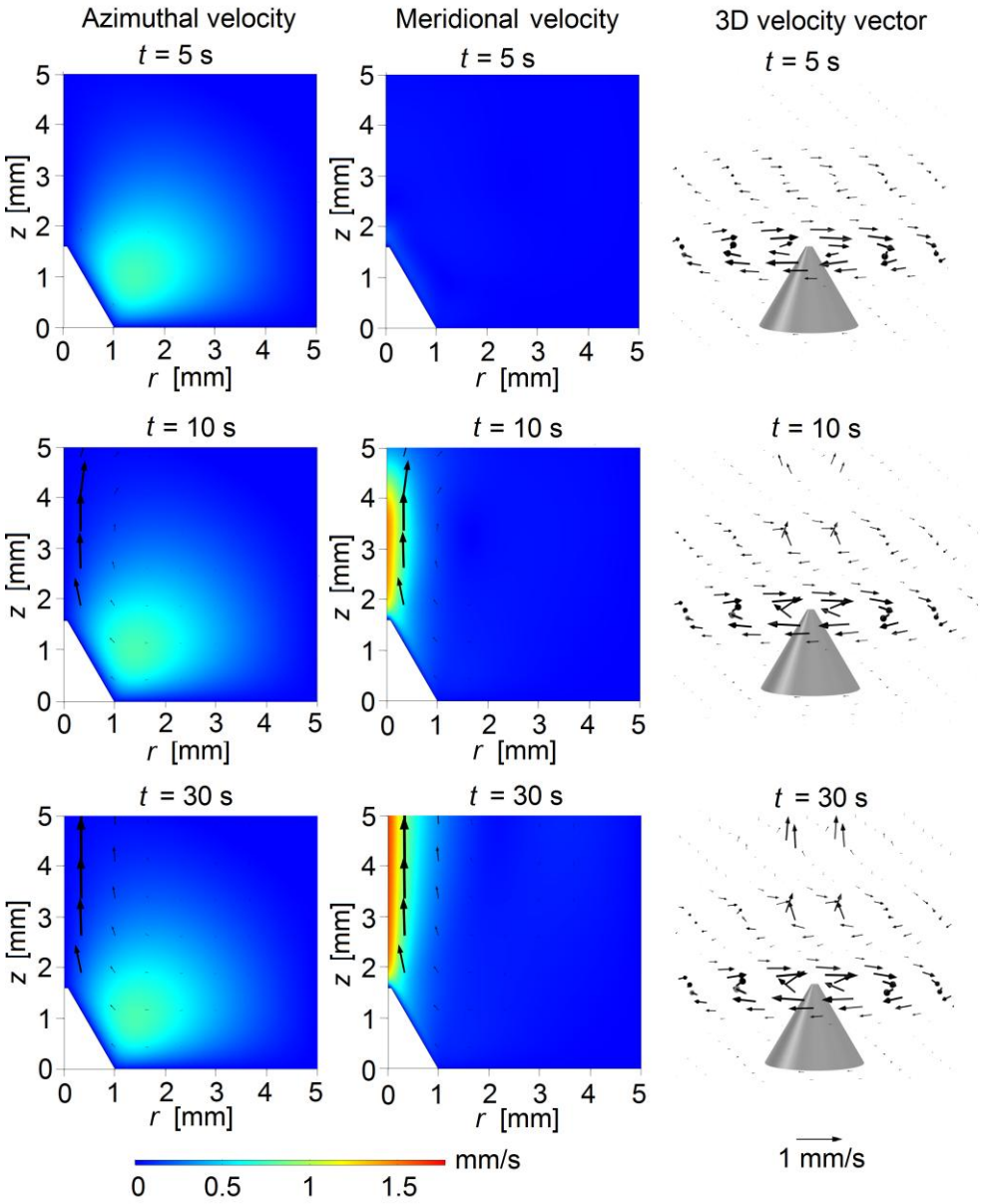

Figure 6: Numerical results of the magnitude of the azimuthal velocity (left) and of the meridional velocity superimposed with the meridional velocity vectors (center), as well as the 3D velocity vectors near the cone (right).

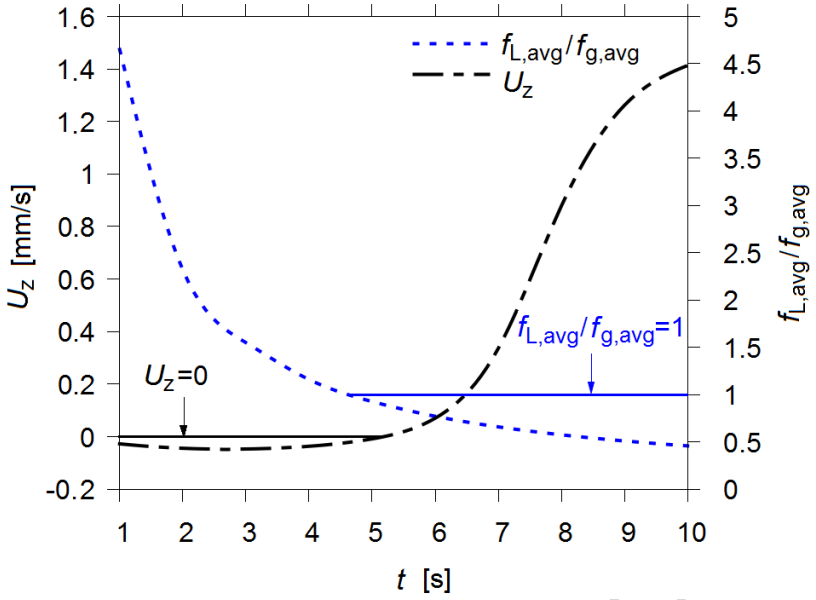

Figure 7: Vertical velocity U_z at a monitoring point 1 mm above the cone tip and the ratio between the spatially averaged Lorentz and buoyancy force (right axis) $f_{L,avg}/f_{g,avg}$ in the start-up phase of the deposition.

The influence of each volume force on the electrolyte flow can be studied in more detail by separately activating the forces in the numerical simulation. **Figure 8** is comparing the vertical velocity along a monitoring line parallel to the slant cone surface at a distance of 0.13 mm from the surface when only the Lorentz force is activated (CufL), only the buoyancy force is activated (Cufg), or both forces are activated (Cu). As shown in **Figure 8** for all instants of time, the Lorentz force alone induces a weak, steady downward flow at the cone. At time 5 s, a weak but already upward directed flow is found in result of both forces, that is counteracted by the Lorentz force, most pronounced in the upper part of the cone. At times 10 s and 30 s, however, the buoyancy force has become so strong that the influence of the Lorentz force can not be recognized anymore, resulting in a distinct upward flow.

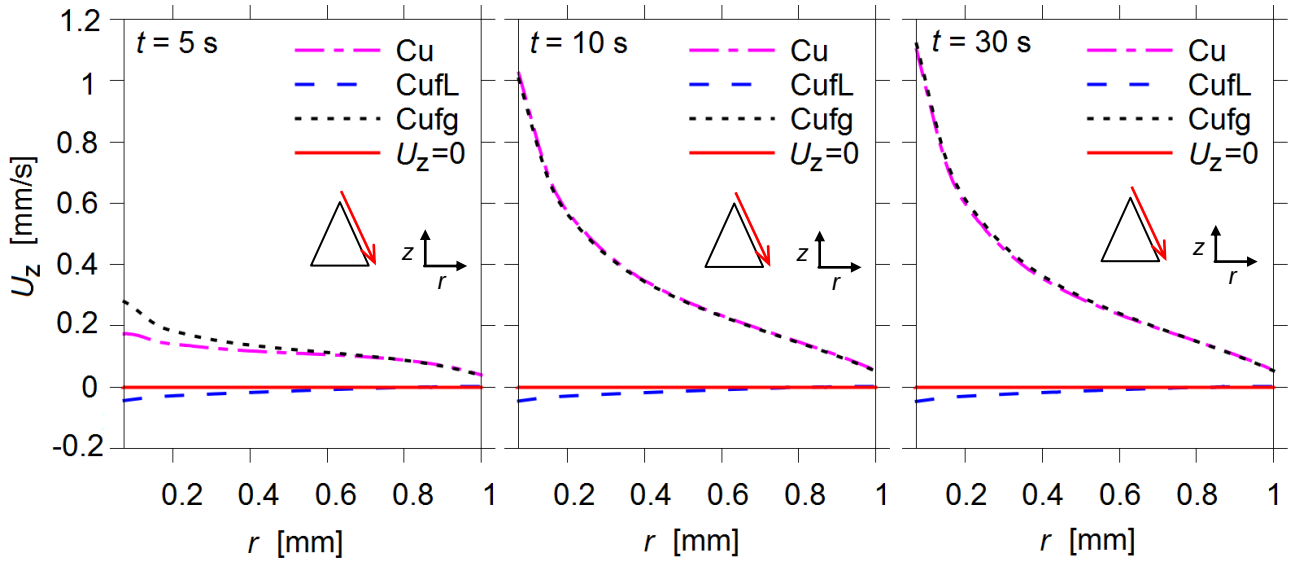

Figure 8: Vertical velocity U_z along a monitoring line at a distance of 0.13 mm from the slant cone surface for 0.075<r<1 mm, when both volume forces are activated (Cu), only the Lorentz force is activated (CufL), or only the buoyancy force is activated (Cufg). A zero velocity line has been added for better comparison. Red arrows indicate the location and the direction of the monitoring line.

Apart from the numerical studies, shadowgraph measurements were conducted to track the path of polysterene particles (size= 36 μm) added to the electrolyte during deposition and to derive information on their velocity. **Figure 9(a)** shows a shadowgraph image with the trajectory of a single particle superimposed in white color. The initial position of the particle at onset of the deposition (x_0=1.75 mm, y_0=0 mm, z_0=0.39 mm) is marked by the white arrow, and the final position shown is reached at t=15 s. The trajectory of the particle was calculated from subsequent shadowgraph images during deposition. Since the cylindrical NdFeB magnet is magnetized vertically downwards, the particle, according to Lorentz force, is moving in clockwise direction around the cone on a spiral path, which may be deduced also from the simulation results shown in **Fig. 6**. The particle is initially located at a position where the azimuthal Lorentz force is predominant and performs almost a complete revolution before it experiences the influence of the cone-parallel buoyant flow developing with time that is lifting up the particle and bringing it closer to the cone. As there the buoyant flow is dominant, eventually the vertical motion is mainly determining its motion, and the particle is leaving the near-cone region close to the symmetry axis of the cone.

Figure 9(b) depicts the temporal behavior of the horizontal in-plane velocity U_x of the particle calculated from its trajectory data. The amplitude of the velocity oscillations that resembles the spiral motion of the particle around the cone described above is decreasing with time accordingly. If the first revolution of the particle around the cone is fitted by a sinusoidal function, an initial period of the azimuthal motion of about 13 s is obtained, with values of the horizontal velocity between -0.49 mm/s and 0.38 mm/s. These values correspond well with the simulation results in **Fig. 6**.

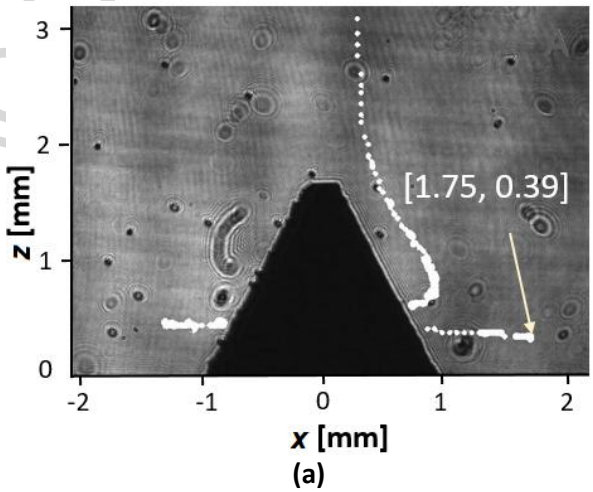

(a)

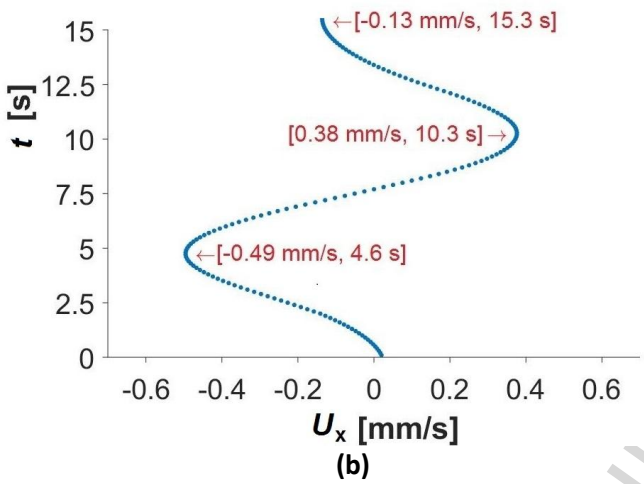

Figure 9: (a) Shadowgraph image of a particle trajectory near the cone. The arrow points to the initial position of the particle when the electrodeposition starts. The path in front of the cone is not shown, as it was hidden by the cone shadow. (b) *x*-component of the particle velocity U_x.

3.3 Simulation results of the structuring effect

In order to evaluate the structuring effect of the magnetic field during electrodeposition on the conical cathode, the deposit thickness at the cone can be calculated from the numerically obtained current density of the axisymmetric simulation [15] [38]:

$$d(r,T) = \frac{V_\mathrm{m}}{zF}\int_0^T j_\mathrm{n}(r,t)\,dt \tag{9}$$

Here T denotes the deposition time, and $V_\mathrm{m} = 7.11 \times 10^{-6}\ \mathrm{m^3/mol}$ is the molar volume of copper. The normal current density and the so-calculated deposit thickness at the cone at different instants of time are presented in **Figure 10** (case NoExtend). Also shown here are the numerical results of a cathode which is extended by a horizontal part of 1.5 millimeter length (case Extend). While the first geometry (case NoExtend), i.e. cathode without extended horizontal part, is originating from the details given in the experimental investigation, the Extend case can be expected to more realistically resemble a planar cathode with several adjacent conical structures. As can be seen, for the cone used in the experiment (NoExtend), the current density is concentrated near the tip and the base of the cone, in agreement with the result of the primary current density distribution at a conical cathode [1]. In the initial phase of the deposition process at 5 s, the diffusion layer is not yet well developed, and the current density is mainly determined by the geometry, yielding a very high current density at the tip of the cone. There might also be a favorable minor influence originating from the downward flow caused by the magnetic field. For later instants of time, as shown above, an upward buoyancy flow is building up, and a thicker concentration boundary layer is appearing at the tip of the cone, which is weakening the local diffusive transport of ions and the associated current density. The deposit at the tip is therefore thinner than at the base of the cone after 10 s and 30 s deposition time in the NoExtend case.

In case of the extended conical cathode, from **Fig. 10** it is clearly seen (case Extend) that the current density remains maximum near the tip of the cone for all instants of time. The current density at the bottom of the cone is much lower than in the NoExtend case, as the cathode now includes a part of the bottom, thus avoiding the current density to peak at the cone base. This allows more current flowing to the tip, resulting in a higher current density there when compared to the NoExtend case. Despite also in the Extend case the upward buoyancy motion along the cone eventually succeeds, the deposit grows fastest at the tip, from which it may be concluded that conical growth is supported in general. However, as it was shown above that the influence of the Lorentz force is mainly limited to the initial phase of the deposition of about $t \leq 5$ s, it can be assumed that this effect is mainly caused by the geometrical aspects of the deposition at the cone.

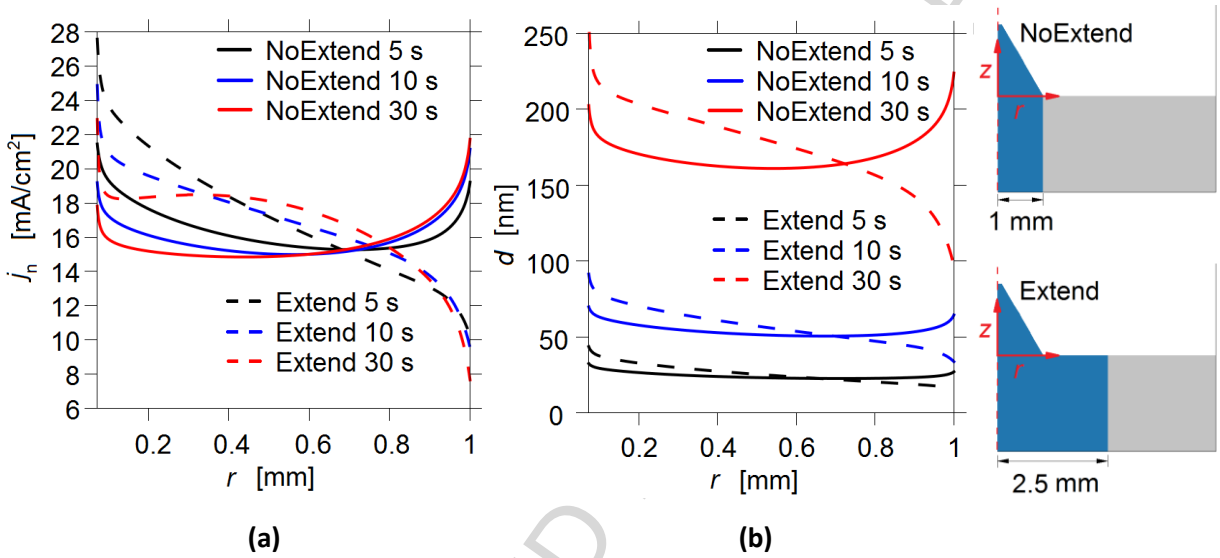

Figure 10: Numerical results of the normal current density j_n (a) and the deposit thickness d (b) along the slant side of the conical cathode (NoExtend) and of the conical part of the extended cathode (Extend), starting at r=0.075 mm (plateau edge of NoExtend case). The averaged current density at the cathode is kept at 16 mA/cm^2 for both cases.

3.4 Influence of the imperfect conical shape

The numerical and experimental results presented so far correspond to a conical cathode, the tip of which is truncated due to fabrication details. In order to quantify the influence of the imperfectness in shape, additional simulations for a cone of perfect shape have been performed. **Figure 11(a)** shows the concentration distribution superimposed with the meridional components of velocity vectors at a time of 30 s near the imperfect (left) and the perfect cone (right). The results are quite similar, except that there is a small area above the terrace of the imperfect cone where the flow is weak. This might be related to buoyancy mainly. At the outer side of the plateau, buoyancy effects from all along the cone surface superimpose and lead to a stronger upward flow than the one generated at the center of the plateau, which may cause a small region of recirculation. Correspondingly, a small variation in the thickness of the concentration boundary layer can be observed for both cases at the plateau height. **Figure 11(b)** shows the

normal current density profiles at both cones for different instants of time. The maximal current density of the perfect cone near the symmetry axis appears exactly at the tip, while for the imperfect cone the current density peaks at the edge of the terrace. The low current density at the terrace is assumed to be related to the weak flow in this region mentioned above. However, these differences are only restricted to the very small tip part of the cone. On the slant side of the cone (x>0.1 mm), the results of the truncated cone and of the perfect cone nicely match. The imperfectness of the cone used in the experiment should therefore not influence the basic results obtained here for the deposition process on conical cathode in a vertical magnetic field.

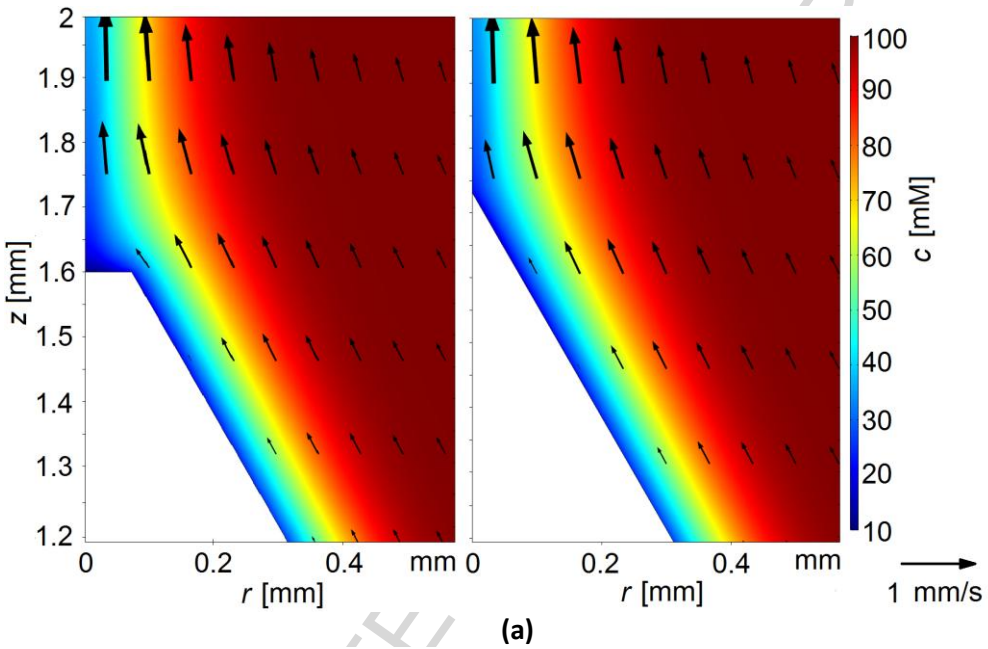

Figure 11: Comparison between the truncated cone and the perfect cone. (a) Concentration distribution c superimposed with the meridional components of the velocity vectors at t=30 s. (b) Normal current density j_n at the imperfect (solid lines) and the perfect cone (dashed lines).

4 Conclusions

The mass transfer and the electrolyte flow near a conically shaped copper electrode under the influence of a vertical magnetic field were investigated numerically and experimentally. The basic motivation for this study arose from the expected beneficial influence of the Lorentz force which is causing a downward-directed secondary flow that might support conical growth. The focus of this work is to understand basic phenomena appearing at a single cone and to study the interplay of the Lorentz and the buoyancy force.

As a result, good qualitative and quantitative agreement between simulations and measurements was found for the copper sulfate concentration of the electrolyte in the vicinity of the cone. For enabling the comparison, the axisymmetric concentration field obtained by the numerical simulations was averaged in the laser direction of the Mach-Zehnder-interferometer. Buoyancy was further found to lead to a delayed onset of an upward flow along the cone surface, that is influencing the thickness of the concentration boundary layer and thereby damping the diffusive transport of ions near the tip of the cone.

Numerical analysis of the electrolyte flow enlighted in detail the interplay of the flow forced by the Lorentz force and by buoyancy. The upward directed buoyancy flow is counteracted by the secondary flow caused by the Lorentz force arising from the vertical magnetic field. However, the favorable effect of the Lorentz force of bringing fresh electrolyte to the tip of the cone is dominant only in the first few seconds of the deposition, after which the flow is mainly determined by the buoyancy force. In the experimental configuration under study, the ratio of both forces was estimated to about 6 % only. A stronger action of the Lorentz force might be achieved by increasing the cell current or by using stronger magnetic fields.

Furthermore, a particle tracking algorithm was applied in shadowgraphy experiments to analyze the electrolyte flow and to visualize the spiral particle motion. The so-calculated flow pattern corresponds qualitatively well with the simulation results.

Despite a cone truncated at its very tip was used in the experiments and simulations, it could be shown that the results at the slant side of the cone are almost not influenced by such a small imperfectness of the shape, which are therefore valid also for perfect cones.

Further numerical simulations at a conical cathode extended radially by a horizontal part avoid the pecularity of the local maximum of the current density at the base of the cone. Such geometry supports conical growth and allows the extension of the results obtained towards cathodes consisting of several cones.

Finally, the delayed onset of the buoyant upward flow compared to the almost instantaneous action of the Lorentz force provides the possibility of maximizing the beneficial influence of the Lorentz force mentioned above by utilizing the different time scales. A natural extension of this work would be to study proper pulsed deposition regimes in the future. Another approach might be to flip the electrochemical cell in order to get rid of the counteracting buoyancy effect that is partly dominating the present configuration. Own future work will be also directed towards the deposition of ferromagnetic metals where additionally magnetic gradient forces are known to become important [16] [38] [39].

Acknowledgements

Financial support by Deutsche Forschungsgemeinschaft, grant no. MU 4209/1-1, EC 201/8-1 and UH 113/3-1 is gratefully acknowledged. The authors thank K. Hennig for the support of the cone preparation.

Declarations of interest

None.

References

[1] C. C. Mcintyre and W. M. Grill, "Finite Element Analysis of the Current-Density and Electric Field Generated by Metal Microelectrodes," *Annals of Biomedical Engineering.,* no. 29, pp. 227-235, 2001.

[2] C. G. Zoski, B. Liu and A. J. Bard, "Scanning Electrochemical Microscopy: Theory and Characterization of Electrodes of Finite Conical Geometry," Analytical Chemistry, no. 76, pp. 3646-3654, 2004.

[3] N. Wang, T. Hang, D. Chu and M. Li, "3D Hierarchical Nanostructured Cu/Ni-Co Coating Electrode for Hydrogen Evolution Reaction," Nano-Micro Lett., no. 7, p. 347, 2015.

[4] K. Brinkert, M. H. Richter, Ö. Akay, J. Liedtke, M. Giersig, K. T. Fountaine and H.-J. Lewerenz, "Efficient solar hydrogen generation in microgravity environment," Nature communications, no. 9, p. 2527, 2018.

[5] H. Matsushima, T. Nishida, Y. Konishi, Y. Fukunaka, Y. Ito and K. Kuribayashi, "Water electrolysis under microgravity Part 1. Experimental technique," Electrochimica Acta, no. 48, pp. 4119-4125, 2003.

[6] S. H. Ahn, S. J. Hwang, S. J. Yoo, I. Choi, H.-J. Kim, J. H. Jang, S. W. Nam, T. H. Lim, T. Lim, S.-K. Kim and J. J. Kim, "Electrodeposited Ni dendrites with high activity and durability for hydrogen evolution reaction in alkaline water electrolysis," Journal of Materials Chemistry, no. 22, p. 15153, 2012.

[7] K. T. Fountaine, H. J. Lewerenz and H. A. Atwater, "Interplay of light transmission and catalytic exchange current in photoelectrochemical system," Applied Physics Letters, no. 105, p. 173901, 2014.

[8] B. Cruz-Ortiz, M. Garcia-Lobato, E. Larios-Durán, E. Múzquiz-Ramos and J. Ballesteros-Pacheco, "Potentiostatic electrodeposition of nanostructured NIO thinfilms for their application as electrocatalyst," Journal of Electroanalytical Chemistry, no. 772, pp. 38-45, 2016.

[9] N. Wang, T. Hang, S. Shanmugam and M. Li, "Preparation and Characterization of Nickel-Cobalt Alloy Nanostructures Array Fabricated by Electrodeposition," Cryst. Eng. Comm., no. 16, pp. 6937-6943, 2014.

[10] M. Uhlemann, K. Tschulik, A. Gebert, G. Mutschke, J. Fröhlich, A. Bund, X. Yang and K. Eckert, "Structured electrodeposition in magnetic gradient fields," The European Physical Journal Special Topics, no. 220, pp. 287-302, 2013.

[11] K. Aoki, "Theory of Current Distribution at a Conical Electrode Under Diffusion Control With Time Dependece," Journal of Electroanalytical Chemistry, no. 281, pp. 29-40, 1990.

[12] M. Chung, P. Gutler, T. Feuchtwang and N. Miskoysky, "Solution of Laplace's Equation for a Rigid Conducting Cone and Planar Counter-Electrode: Comparison With the Solution to the Taylor Conical Model of a Field Emission LMIS," Journal de Physique Colloques, no. 45, pp. C9-145-C9-152, 1984.

[13] D. Britz, S. Chandra, J. Strutwolf and D. K. Y. Wong, "Diffusion-limited Chronoamperometry at Conical-tip Microelectrodes," Electrochimica Acta, no. 55, pp. 1272-1277, 2010.

[14] R. Aogaki, K. Fueki and T. Mukaibo, "Application of magnetohydrodynamic effect to the analysis of electrochemical reactions.," Denki Kagaku, no. 43, p. 504/509, 1975.

[15] S. Mühlenhoff, G. Mutschke, U. Uhlemann, X. Yang, S. Odenbach, J. Fröhlich and K. Eckert, "On the

homogenization of the thickness of Cu deposits by means of MHD convection within small dimension cells.," Electrochemistry Communications, no. 36, pp. 80-83, 2013.

[16] G. Mutschke, K. Tschulik, T. Weier, M. Uhlemann, A. Bund and J. Fröhlich, "On the Action of Magnetic Gradient Forces in Micro-structured Copper Deposition," Electrochimica Acta, no. 55, pp. 9060-9066, 2010.

[17] G. Mutschke, A. Hess, A. Bund and J. Fröhlich, "On the origin of horizontal counter-rotating electrolyte flow during copper magnetoelectrolysis," Electrochimica Acta, no. 55, pp. 1543-1547, 2010.

[18] K. M. Grant, J. W. Hemmert and H. S. White, "Magnetic field driven convective transport at inlaid disk microelectrodes: The dependence of flow patterns on electrode radius," Journal of Electroanalytical Chemistry, no. 500, pp. 95-99, 2001.

[19] K. Tschulik, X. Yang, G. Mutschke, M. Uhlemann, K. Eckert, R. Sueptitz, L. Schultz and A. Gebert, "How to Obtain Structured Metal Deposits from Diamagnetic Ions in Magnetic Gradient Fields?," Electrochemistry Communications, no. 13, pp. 946-950, 2011.

[20] F. Karnbach, M. Uhlemann, A. Gebert, J. Eckert and K. Tschulik, "Magnetic Field Templated Patterning of the Soft Magnetic Alloy CoFe," Electrochimica Acta, no. 123, pp. 477-484, 2014.

[21] P. E. Strizhak, "Nanosize Effects in Heterogeneous Catalysis," Theoretical and Experimental Chemistry, no. 49, pp. 2-21, 2013.

[22] A. Heinze, K. Eckert, M. J. Hauser and S. Odenbach, "A wavelet and Zernike-polynomial-based shearing interferometry approach to analyse hydrodynamic instabilities at interfaces," Acta Astronautica, no. 68, pp. 707-716, 2011.

[23] Z. Lei, X. Yang, C. Haberstroh, B. Pulko, S. Odenbach and K. Eckert, "Space- and time-resolved interferometric measurements of the thermal boundary layer at a periodically magnetized gadolinium plate," International Journal of Refrigeration, no. 56, pp. 246-255, 2015.

[24] Z. Lei, B. Fritzsche and K. Eckert, "Evaporation-assisted magnetic separation of rare-earth ions in aqueous solutions," Journal of Physical Chemistry, no. 44, pp. 24576-24587, 2017.

[25] Z. Lei, C. Haberstroh, S. Odenbach and K. Eckert, "Heat transfer enhancement in magnetic cooling by means of magnetohydrodynamic convection," International Journal of Refrigeration, no. 62, pp. 166-176, 2016.

[26] G. Marinaro, R. La Rocca, A. Toma, M. Barberio, L. Cancedda, E. Di Fabrizio, P. Decuzzi and F. Gentile, "Networks of neuroblastoma cells on porous silicon subtrates reveal a small world topology," Integrative Biology, no. 7, pp. 184-197, 2014.

[27] D. R. Lide, CRC Handbook of Chemistry and Physics, Boca Raton, FL: CRC Press, 2005.

[28] D. Koschichow, G. Mutschke, X. Yang, A. Bund and J. Froehlich, "Numerical Simulation of the Onset of Mass Transfer and Convection in Copper Electrolysis Subjected to a Magnetic Field," Russian Jounal of Electrochemistry, no. 48, pp. 682-691, 2012.

[29] J. Newman and K. E. Thomas-Alyea, Electrochemical Systems, 3 ed., Hoboken, New Jersey: John Wiley and Sons, 2004.

[30] V. Marathe and J. Newman, "Current distribution on a rotating disk electrode," Journal of the Electrochemical Society, no. 116, pp. 1704-1707, 1969.

[31] J. P. Chopart, J. Douglade, P. Fricoteaux and A. Olivier, "Electrodeposition and electrodissolution of copper with a magnetic field: dynamic and stationary investigations," Electrochemica Acta, no. 36, pp. 459-463, 1991.

[32] T. Hurlen, "On the kinetics of the Cu/Cuaq++ electrode," Acta Chemica Scandivanica, no. 15, pp. 630-644, 1961.

[33] E. Mattsson and J. O. Bockris, "Galvanostatic studies of the kinetics of deposition and dissolution in the copper+copper sulphate system," Transactions of the Faraday Society, no. 55, pp. 1586-1601, 1959.

[34] J. Newman, "Current distribution on a rotating disk below the limiting current," Journal of the Electrochemical Society, no. 113, pp. 1235-1241, 1966.

[35] COMSOL, COMSOL Multiphysics Documentation Suite V.5.3.a, Burlington, MA 01803, USA, 2018.

[36] N. H. Abel, "Auflösung einer mechanischen Aufgabe," Journal für die reine und angewandte Mathematik, no. 1, pp. 153-157, 1826.

[37] X. Yang, K. Eckert, A. Heinze and M. Uhlemann, "The concentration field during transient natural convection between vertical electrodes in a small-aspect-ratio," Journal of Electroanalytical Chemistry, no. 613, pp. 97-107, 2008.

[38] G. Mutschke, K. Tschulik, M. Uhlemann, A. Bund and J. Fröhlich, "Comment on "Magnetic structuring of electrodeposits"," Physical Review Letters, no. 109, p. 229401, 2012.

[39] K. Tschulik, C. Cierpka, G. Mutschke, A. Gebert, L. Schultz and M. Uhlemann, "Clarifying the Mechanism of Reverse Structuring during Electrodeposition in Magnetic Gradient Fields," Analytical chemistry, no. 84, pp. 2328-2334, 2012.

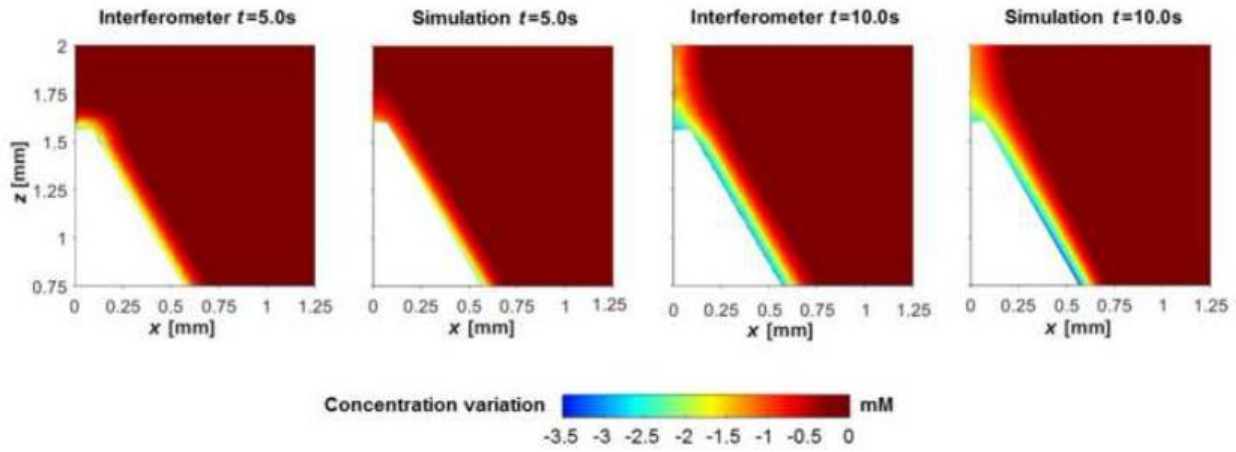

Graphical abstract

Highlights

- combined experimental and numerical study of the electrodeposition of copper at a conically shaped electrode
- the single cone study is motivated as generic case of rough and regularly surface-structured electrodes
- a vertical magnetic field is found to be beneficial for enhancing conical growth
- the secondary flow induced by the Lorentz force increases the deposition rate near the cone tip
- the influence of buoyancy caused by the electrode reaction is strong and superimposing the magnetic field effect, but might be mitigated by different means